

SANDIA REPORT

SAND2008-1782

Unlimited Release

Printed March 2008

Computational Design and Analysis of Flatback Airfoil Wind Tunnel Experiment

C.P. "Case" van Dam, Edward A. Mayda, David D. Chao, Dale E. Berg

Prepared by
Sandia National Laboratories
Albuquerque, New Mexico 87185 and Livermore, California 94550

Sandia is a multiprogram laboratory operated by Sandia Corporation,
a Lockheed Martin Company, for the United States Department of Energy's
National Nuclear Security Administration under Contract DE-AC04-94AL85000.

Approved for public release; further dissemination unlimited.



Issued by Sandia National Laboratories, operated for the United States Department of Energy by Sandia Corporation.

NOTICE: This report was prepared as an account of work sponsored by an agency of the United States Government. Neither the United States Government, nor any agency thereof, nor any of their employees, nor any of their contractors, subcontractors, or their employees, make any warranty, express or implied, or assume any legal liability or responsibility for the accuracy, completeness, or usefulness of any information, apparatus, product, or process disclosed, or represent that its use would not infringe privately owned rights. Reference herein to any specific commercial product, process, or service by trade name, trademark, manufacturer, or otherwise, does not necessarily constitute or imply its endorsement, recommendation, or favoring by the United States Government, any agency thereof, or any of their contractors or subcontractors. The views and opinions expressed herein do not necessarily state or reflect those of the United States Government, any agency thereof, or any of their contractors.

Printed in the United States of America. This report has been reproduced directly from the best available copy.

Available to DOE and DOE contractors from
U.S. Department of Energy
Office of Scientific and Technical Information
P.O. Box 62
Oak Ridge, TN 37831

Telephone: (865) 576-8401
Facsimile: (865) 576-5728
E-Mail: reports@adonis.osti.gov
Online ordering: <http://www.osti.gov/bridge>

Available to the public from
U.S. Department of Commerce
National Technical Information Service
5285 Port Royal Rd.
Springfield, VA 22161

Telephone: (800) 553-6847
Facsimile: (703) 605-6900
E-Mail: orders@ntis.fedworld.gov
Online order: <http://www.ntis.gov/help/ordermethods.asp?loc=7-4-0#online>



SAND2008-1782
Unlimited Release
Printed March 2008

Computational Design and Analysis of Flatback Airfoil Wind Tunnel Experiment

C.P. "Case" van Dam, Edward A. Mayda, and David D. Chao
Department of Mechanical and Aeronautical Engineering
University of California
One Shields Avenue
Davis, CA 95616-5294

Dale E. Berg, Sandia National Laboratories Technical Manager

Sandia Contract No. 15890

Abstract

A computational fluid dynamics study of thick wind turbine section shapes in the test section of the UC Davis wind tunnel at a chord Reynolds number of one million is presented. The goals of this study are to validate standard wind tunnel wall corrections for high solid blockage conditions and to reaffirm the favorable effect of a blunt trailing edge or flatback on the performance characteristics of a representative thick airfoil shape prior to building the wind tunnel models and conducting the experiment. The numerical simulations prove the standard wind tunnel corrections to be largely valid for the proposed test of 40% maximum thickness to chord ratio airfoils at a solid blockage ratio of 10%. Comparison of the computed lift characteristics of a sharp trailing edge baseline airfoil and derived flatback airfoils reaffirms the earlier observed trend of reduced sensitivity to surface contamination with increasing trailing edge thickness.

Acknowledgements

This project was supported by TPI Composites of Warren, Rhode Island under Contract 15890 – Revision 4 with Sandia National Laboratories. The primary members of the TPI team were Derek Berry (Principal Investigator) and Steve Nolet of TPI, Kevin Jackson of Dynamic Design, Michael Zuteck of MDZ Consulting and C.P. (Case) van Dam and his graduate students (Edward Mayda and David Chao for this particular effort) at the University of California at Davis. The members of the Sandia team were Tom Ashwill, Dale Berg (Technical Manager), Daniel Laird, Mark Rumsey, Herbert Sutherland, Paul Veers and Jose Zayas.

Table of Contents

Abstract.....	3
Acknowledgements	4
Table of Contents	5
List of Figures.....	6
List of Tables	8
Introduction.....	9
Airfoils.....	10
Computational Methods.....	11
MSES	11
ARC2D	12
OVERFLOW	13
Turbulence Model.....	13
Computational Grids	13
Results and Discussion.....	15
TR Section Shapes	16
FB Section Shapes	21
Discussion.....	24
Conclusions.....	25
References.....	32

List of Figures

Figure 1	Blade section geometries for the baseline TR-4000-0050 and its derivative flatback sections: TR-4000-1000 and TR-4000-2000.	10
Figure 2	Blade section geometries for the baseline FB-4000-0050 and its derivative flatback sections: FB-4000-1000 and FB-4000-2000.	11
Figure 3	Grid approach for the unbounded flow cases: (a) overall view of the O-grid for the TR-4000-0050 section where the farfield boundary is nominally 50 chord lengths from the airfoil surface (some radial gridlines omitted for clarity) and (b) detail view of the O-grid near the airfoil surface.	14
Figure 4	Grid approach for the wind tunnel cases: (a) overall view showing test section, diffuser and airfoil model (some gridlines omitted for clarity), (b) view of TR-4000-2000 mesh at 10° angle of attack and its overlap region with the tunnel grid, and (c) detail view of model wake region showing overlap of the airfoil model and tunnel grids.	14
Figure 5	MSES lift predictions for TR-4000-0050 with and without wind tunnel walls at $Re = 1.0$ million and transition free and transition fixed at 5% of the chord on upper and lower surface. The lift curve labeled corrected is obtained by applying standard wind tunnel wall corrections [4] to the with wind tunnel wall results.	16
Figure 6	OVERFLOW lift predictions for TR-4000-0050 with and without wind tunnel walls at $Re = 1.0$ million and transition fixed at 5% of the chord on upper and lower surface. The lift curve labeled corrected is obtained by applying standard wind tunnel wall corrections [4] to the with wind tunnel wall results.	17
Figure 7	OVERFLOW drag predictions for TR-4000-0050 with and without wind tunnel walls at $Re = 1.0$ million and transition fixed at 5% of the chord on upper and lower surface. The lift curve labeled corrected is obtained by applying standard wind tunnel wall corrections [4] to the with wind tunnel wall results.	18
Figure 8	MSES lift predictions for TR-4000-1000 with and without wind tunnel walls at $Re = 1.0$ million and transition free and transition fixed at 5% of the chord on upper and lower surface. The lift curve labeled corrected is obtained by applying standard wind tunnel wall corrections [4] to the with wind tunnel wall results.	18

Figure 9	OVERFLOW lift predictions for TR-4000-1000 with and without wind tunnel walls at $Re = 1.0$ million and transition free and transition fixed at 5% of the chord on upper and lower surface. The lift curve labeled corrected is obtained by applying standard wind tunnel wall corrections [4] to the with wind tunnel wall results.	19
Figure 10	OVERFLOW drag predictions for TR-4000-1000 with and without wind tunnel walls at $Re = 1.0$ million and transition free and transition fixed at 5% of the chord on upper and lower surface. The lift curve labeled corrected is obtained by applying standard wind tunnel wall corrections [4] to the with wind tunnel wall results.	20
Figure 11	OVERFLOW lift predictions for TR-4000-2000 with and without wind tunnel walls at $Re = 1.0$ million and transition free and transition fixed at 5% of the chord on upper and lower surface. The lift curve labeled corrected is obtained by applying standard wind tunnel wall corrections [4] to the with wind tunnel wall results.	20
Figure 12	OVERFLOW drag predictions for TR-4000-2000 with and without wind tunnel walls at $Re = 1.0$ million and transition free and transition fixed at 5% of the chord on upper and lower surface. The lift curve labeled corrected is obtained by applying standard wind tunnel wall corrections [4] to the with wind tunnel wall results.	21
Figure 13	MSES and ARC2D lift predictions for FB-4000-0050 with transition free and transition fixed at 5% of the chord on upper and lower surface.	22
Figure 14	MSES and ARC2D drag predictions for FB-4000-0050 with transition free and transition fixed at 5% of the chord on upper and lower surface.	22
Figure 15	MSES and ARC2D lift predictions for FB-4000-1000 with transition free and transition fixed at 5% of the chord on upper and lower surface.	23
Figure 16	MSES and ARC2D drag predictions for FB-4000-1000 with transition free and transition fixed at 5% of the chord on upper and lower surface.	23
Figure 17	ARC2D lift predictions for FB-4000-2000 with transition free and transition fixed at 5% of the chord on upper and lower surface.	24
Figure 18	ARC2D drag predictions for FB-4000-2000 with transition free and transition fixed at 5% of the chord on upper and lower surface.	24

List of Tables

Table 1	TR-4000-0050 coordinates	26
Table 2	TR-4000-1000 coordinates	27
Table 3	TR-4000-2000 coordinates	28
Table 4	FB-4000-0050 coordinates.....	29
Table 5	FB-4000-1000 coordinates.....	30
Table 6	FB-4000-2000 coordinates.....	31

Introduction

Blunt trailing edge or flatback airfoils have been proposed for the inboard region of large wind turbine blades [1,2,3]. Flatback airfoils provide several structural and aerodynamic performance advantages. Structurally, the flatback increases the sectional area and sectional moment of inertia for a given airfoil maximum thickness [1]. Aerodynamically, the flatback increases sectional maximum lift coefficient and lift curve slope and reduces the well-documented sensitivity of thick airfoils to surface soiling [3].

Limited experimental data are available that validate the aerodynamic performance benefits of the blunt trailing edge concept for thick airfoils. This lack of experimental data in the open literature has led to the request to conduct a wind tunnel study on the effect of the blunt trailing edge on the aerodynamic characteristics of a thick blade section with free and fixed transition at representative Reynolds numbers. A maximum thickness to chord ratio (t/c) of 40% was selected for this experiment because it is at the high end of section shape thickness considered for the root region of wind turbine blades. One of the problems with wind tunnel testing thick airfoils is that these types of models tend to create a significant amount of solid blockage (ratio of frontal area of the model to the test section cross-sectional area) and wake blockage (size of model wake relative to that of test section) thereby affecting the flow development in the wind tunnel test section. Solid blockage is typically kept at 5% or less, but this value limits the model chord length, which in turn limits the chord Reynolds numbers [4]. Here we plan to acquire data on $t/c = 0.40$ airfoils at chord Reynolds numbers greater than or equal to one million in the UC Davis tunnel. This Reynolds number can be achieved by testing a model with a 12-in. chord at an airspeed of 107 mph and standard sea-level conditions. This model selection leads to a solid blockage ratio of 10% (model maximum thickness of 0.4 ft and test section width of 4 ft). The question arises to what extent this level of blockage affects the data and if the standard wind tunnel wall corrections [4] are adequate to correct the measured data. A series of computational fluid dynamics simulations were conducted to analyze the performance characteristics of a series of thick airfoils with and without wind tunnel walls at a Reynolds number of one million.

In the following section, two airfoil series considered for this wind tunnel study are presented. The FB airfoil series developed in Phase I of the Blade System Design Study (BSDS) [2] and the TR airfoil series presented and discussed in [3]. Next, the computational methods and grids are introduced. The performance characteristics of the airfoils are computationally investigated with and without wind tunnel walls at the proposed flow conditions. Wind tunnel wall corrections are applied to computational results obtained with walls. The corrected data are then compared with the unbounded flow results.

Airfoils

In their study of blunt trailing edge airfoils, Standish & van Dam focused on $t/c = 35\%$ airfoils of the TR series. To better match the maximum thickness values presently found on the inboard sections of large turbine blades, $t/c = 40\%$ airfoils are proposed for the wind tunnel experiment. Depicted in Fig. 1 is the TR-4000-0050; the baseline airfoil with a nominally sharp trailing edge. It is derived from the S821 section shape, but the TR-4000-0050 has a maximum thickness to chord ratio of 40%. Also, as indicated in Table 1, the actual trailing edge thickness to chord ratio of this airfoil is not zero but 0.5% (0.06 in. based on a one-foot chord model). The reasons for the finite trailing edge thickness are twofold. Physically, any blade section or wind tunnel model will have a finite trailing edge thickness and it is good practice to incorporate this attribute in the design and analysis from the onset. Computationally, a zero trailing edge thickness airfoil dictates a different grid topology than a finite trailing edge thickness airfoil and it is preferred to minimize grid changes when comparing computed results of sharp and blunt trailing edge airfoils.

The TR-4000-1000 has the identical maximum thickness as the TR-4000-0050 but has a trailing-edge thickness of 10% as shown in Fig. 1 and Table 2. The blunt trailing edge is created by symmetrically adding thickness to either side of the camber line of the TR-4000-0050 using an exponential blending function to smoothly distribute the increased thickness along the chord.

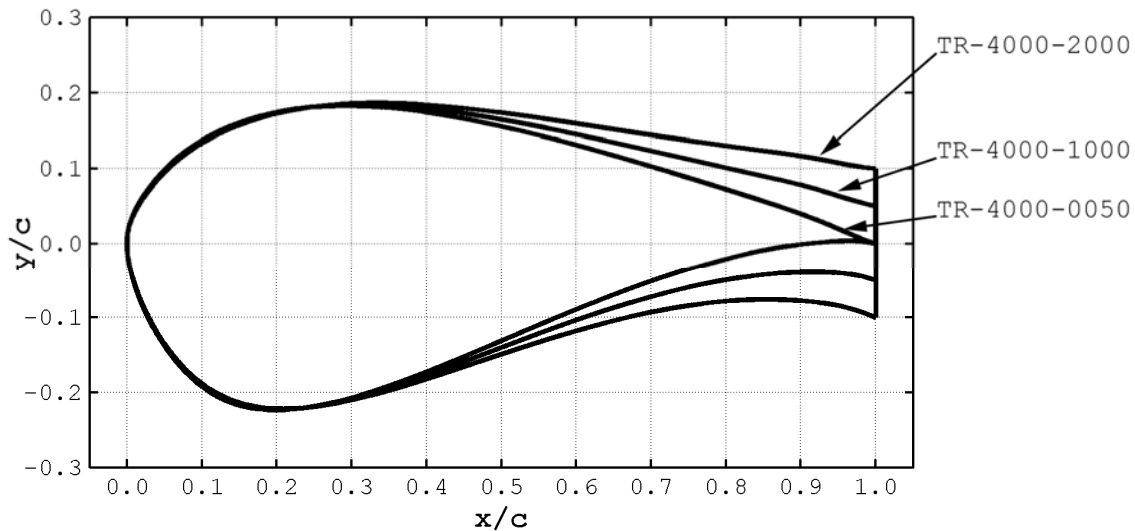


Figure 1 Blade section geometries for the baseline TR-4000-0050 and its derivative flatback sections: TR-4000-1000 and TR-4000-2000.

The TR-4000-2000 has the identical maximum thickness as the TR-4000-0050 and the TR-4000-1000 but has a trailing-edge thickness of 20% as shown in Fig. 1 and Table 3. The blunt trailing edge is created as described above. Note that for this airfoil the difference between the maximum thickness and trailing edge thickness $(t - t_{te})/c = 20\%$.

Sharp trailing edge airfoils of this thickness (such as the S821, $t/c = 0.24$) can be designed to have lift characteristics that are largely insensitive to surface soiling. A simple design guideline for blunt trailing edge or flatback airfoils is to limit the ratio of the difference between maximum thickness and trailing edge thickness and the chord length to 20-25% to make surface insensitive lift characteristics achievable. Based on this rule-of-thumb one would expect to see significant sensitivity to surface soiling for the TR-4000-1000 and little or no sensitivity for the TR-4000-2000.

A second airfoil family considered for experimental evaluation is the FB series presented in the final report of Phase I of the Blade System Design Study (BSDS) [2]. This series of airfoil shapes was generated by combining a low-pressure side shape drawn from the thick, high lift inboard NREL airfoils, and a structurally efficient high-pressure side drawn from the LS-1 series airfoils. Depicted in Fig. 2 are the FB-4000-0050, the FB-4000-1000, and the FB-4000-2000 whereas the surface coordinates for these three airfoils are presented in Tables 4 through 6. Note that the FB-4000-1000 with its maximum thickness to chord ratio (t/c) of 40% and trailing edge thickness to chord ratio (t_{te}/c) of 10% closely matches the FB-4286-0802 ($t/c = 42.86\%$ and $t_{te}/c = 8.02\%$) section shape applied in BSDS Phase I [2].

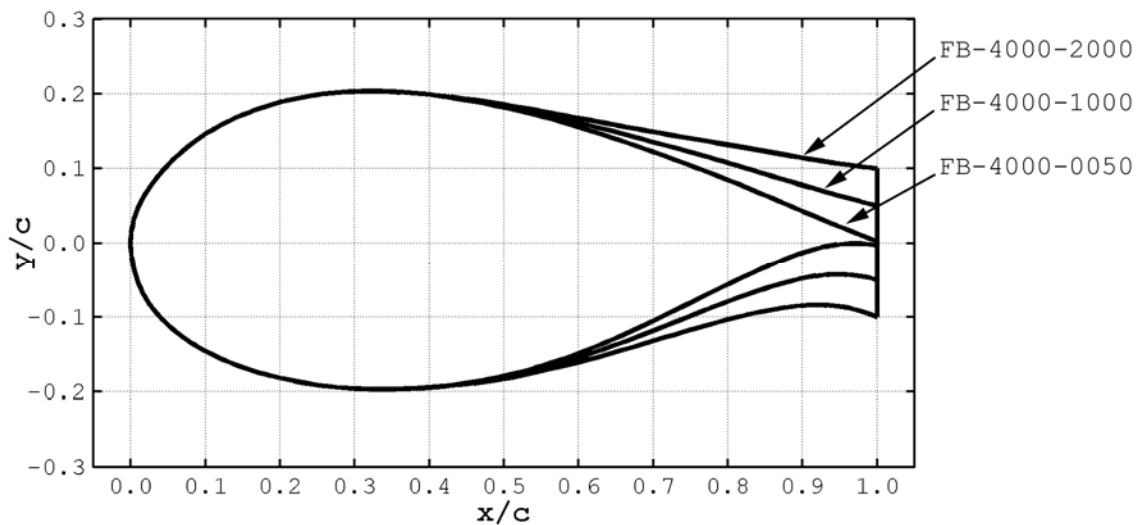


Figure 2 Blade section geometries for the baseline FB-4000-0050 and its derivative flatback sections: FB-4000-1000 and FB-4000-2000.

Computational Methods

MSES

The MSES flow solver developed by M. Drela [5,6] at MIT is based upon a viscous/inviscid zonal interaction method. The inviscid region is modeled using the Euler equations and the viscous region is modeled by a compressible lag-dissipation integral method. The viscous and inviscid zones are coupled through the boundary-layer

displacement thickness on the inviscid flow and the boundary-layer edge velocity on the viscous flow. This approach yields a non-linear coupled system of equations that can be solved using a global Newton solution procedure. As a result, this code is relatively simple and solutions converge rapidly. MSES comes with its own grid generation tool called MSET, which constructs an initial grid based on inviscid streamlines. Once the calculation is initiated, the streamline grid itself is part of the solution and therefore is updated after each successive iteration. Two very useful tools, called MPLOT and MEDP, are included and provide aid in post-processing. MPLOT is a plotting tool capable of plotting a large number of parameters pertinent to the flow solution. MEDP is a tool that Drela refers to as “an airfoil redesign system rather than a pure design system”, since it requires that a converged solution be obtained prior to its execution. MEDP was primarily used to extract the surface pressure and skin friction distributions.

MSES incorporates several boundary conditions which coincide with the presence of wind tunnel walls or an unbounded domain. For the wind tunnel cases, a solid wall is specified as the farfield boundary condition, and the distance to the walls is specified separately to coincide with the nondimensional ratios relative to the test model. For an unbounded domain, application of potential theory to an airfoil’s aerodynamic center is used to apply a superposition of potential vortex, source, and two doublet components for the farfield boundary condition. The distance to the farfield for this case is then not constrained, since this boundary condition should be applicable to any farfield distance.

At this point, MSES is paramount in the blunt trailing edge study because it incorporates a boundary layer transition model. The transition prediction model used in MSES is referred to as the “envelope method”, which is a simplified version of the e^n method. Due to the lack of transition prediction models in the Reynolds-averaged Navier-Stokes (RaNS) solvers, all RaNS free transition results in this study are, in fact, results obtained with transition specified at the locations predicted by MSES. An additional advantage of this procedure is that it minimizes discrepancies in the aerodynamic performance predictions of the various computational methods as a result of differences in transition location. MSES includes a model for blunt trailing edge flows [6]. However, there is some concern about the accuracy of this model for any trailing edge thickness in excess of a few percent. This spurred the use of methods based on the Reynolds-averaged Navier-Stokes equations.

ARC2D

ARC2D was developed by T. Pulliam and J. Steger [7,8] at the NASA Ames Research Center. The code solves the compressible, two-dimensional, Reynolds-averaged Navier-Stokes equations in strong conservation-law form. The governing equations in generalized curvilinear coordinates are central differenced in standard second-order form and solved using the implicit Beam-Warming approximate factorization scheme [9]. Artificial dissipation terms are added for numerical stability with the 2nd order dissipation coefficient = 0.00 and the 4th order dissipation coefficient = 0.64. The code employs local time stepping and mesh sequencing to accelerate convergence of steady solutions.

ARC2D has been extensively applied to analyze inviscid and viscous flows over airfoils [7,10,11,12].

OVERFLOW

OVERFLOW is a three-dimensional, compressible RaNS flow solver developed by Buning, Jespersen, Pulliam, Chan, Slotnick, Krist, and Renze at NASA [13]. Use of three identical computational planes in the spanwise direction permits the modeling of two-dimensional flows. The use of OVERFLOW allows for the future extension of this study to three-dimensional flows. Steady and time-accurate solutions can be calculated on structured block or Chimera overset grids. In this study, all computations are time-accurate and conducted with a central-differencing block tri-diagonal scheme. Dual time-stepping is utilized to obtain 2nd order accuracy in time. Artificial dissipation (2nd order dissipation coefficient = 0.00; 4th order dissipation coefficient = 0.04) is used to aid numerical stability. A recent application of this method to study bubble-induced unsteadiness on wind turbine airfoils is presented by Mayda and van Dam [14].

Turbulence Model

Two different turbulence models are employed. The first is the one-equation Spalart-Allmaras (SA) model [15] used in ARC2D and the second is a two-equation $k-\omega$ shear stress transport model due to Menter (SST) [16] used in OVERFLOW. Both models are linear eddy viscosity models that employ the Boussinesq eddy viscosity assumption.

Computational Grids

All meshes for the RaNS calculations in this study were generated with the Chimera Grid Tools and OVERGRID codes developed by Chan, Rogers, Nash, Buning and Meakin [17] at the NASA Ames Research Center. All airfoil grids are of the O-grid variety shown in Fig. 3. For unbounded flow cases, the grid domain extends roughly 50 chord lengths from the airfoil surface. A freestream/characteristic boundary condition is imposed at the outer edge of this domain, and a no-slip condition is specified at the airfoil surface. For wind tunnel cases, a Chimera overset grid approach was employed. The tunnel interior, including test section and diffuser, was discretized with a stretched Cartesian mesh as shown in Fig. 4a. The airfoil model grid was then placed inside the tunnel test section at the appropriate angle of attack (see Fig. 4b). Flowfield information is shared between the two grids via interpolation in the overlap region, an example of which is shown in Fig. 4c. The tunnel walls were modeled with an inviscid solid surface boundary condition. At the tunnel inlet, an imposed freestream condition was used, whereas a specified mass flow boundary condition was applied at the tunnel exit plane.

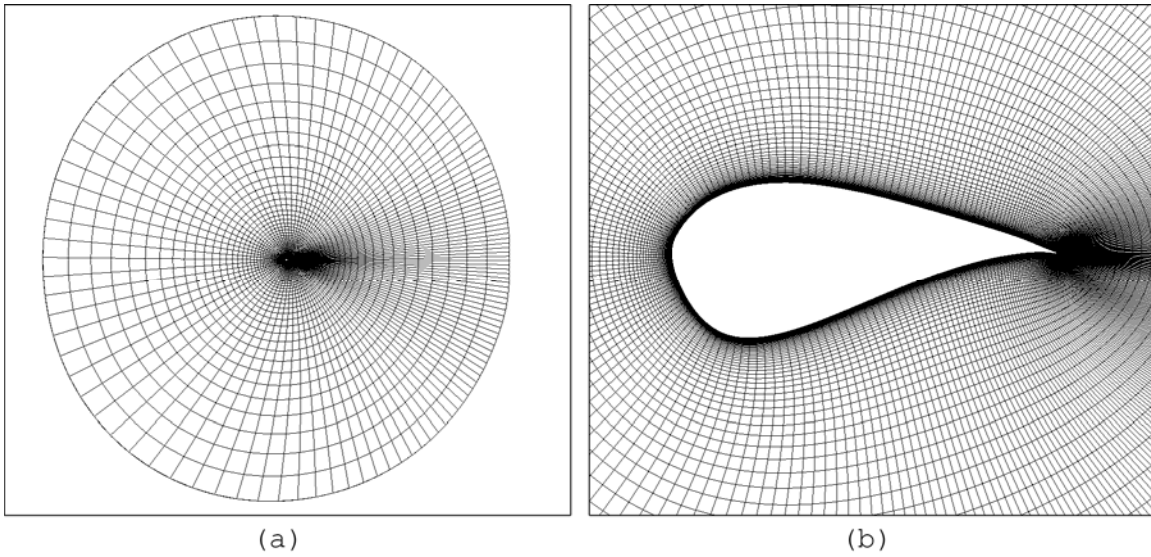


Figure 3 Grid approach for the unbounded flow cases: (a) overall view of the O-grid for the TR-4000-0050 section where the farfield boundary is nominally 50 chord lengths from the airfoil surface (some radial gridlines omitted for clarity) and (b) detail view of the O-grid near the airfoil surface.

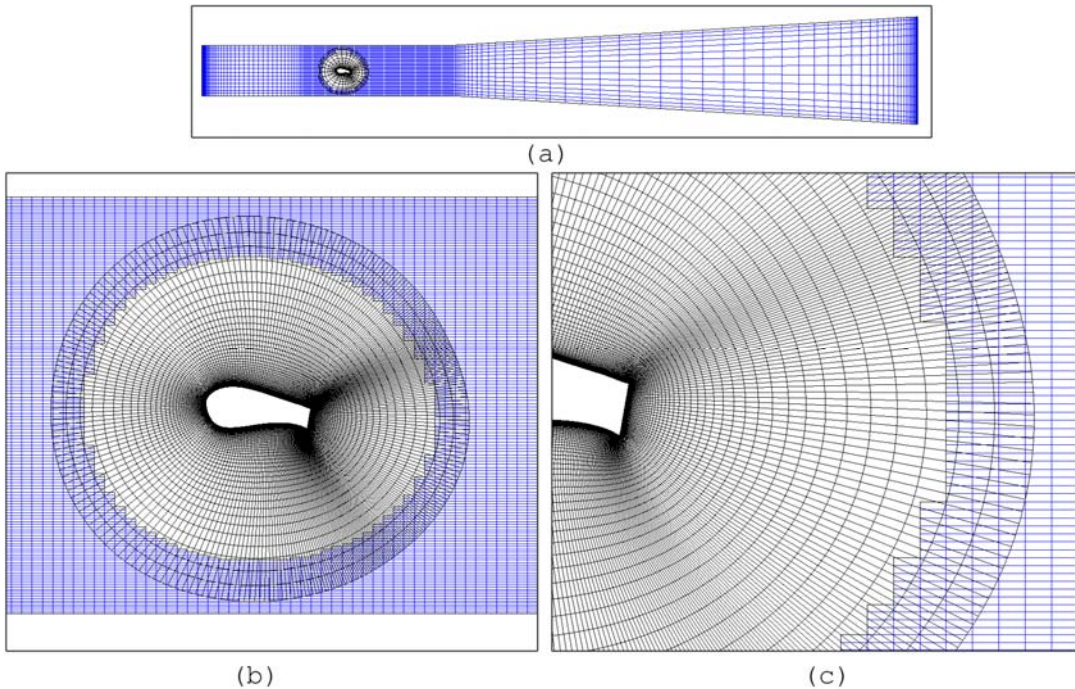


Figure 4 Grid approach for the wind tunnel cases: (a) overall view showing test section, diffuser and airfoil model (some gridlines omitted for clarity), (b) view of TR-4000-2000 mesh at 10° angle of attack and its overlap region with the tunnel grid, and (c) detail view of model wake region showing overlap of the airfoil model and tunnel grids.

Results and Discussion

Before presenting and discussing the numerical prediction it is useful to review the corrections that are applied to wind tunnel results for airfoils. The two-dimensional wall corrections applied to the wind tunnel data, whether from numerical modeling or experimental wind tunnel testing, consist of three factors: solid blockage, wake blockage, and streamline curvature.

Solid blockage comes from the presence of the model itself in the wind tunnel test section. Because this presence reduces the cross-sectional area of the tunnel, the air flow velocity is increased over the model. This effect is a function of model thickness, thickness distribution, and model size, but is not a function of camber. There are numerous methods to account for solid blockage, but the form given by Thom (see [4]) is used due to its clearer expression of the parameters producing solid blockage. Thom's equation is given as:

$$\epsilon_{sb} = \frac{K_l \times Vol}{C^{\frac{3}{2}}}$$

where $K_l = 0.52$ for a test model spanning the tunnel height, Vol is the model volume, and C is the tunnel cross-sectional area.

The second factor in wall corrections is wake blockage. A body in flow will leave a wake behind. The mean velocity of the wake will be lower than the freestream velocity. By continuity, this also means the velocity outside the wake will have a higher velocity to conserve the volume flow. These velocity differences result in a pressure gradient which increases the air flow over the model. From [4], Maskell's correction for wake blockage is used and is given as:

$$\epsilon_{wb} = \frac{c/h}{2} c_{du}$$

where c is the chord length of the airfoil, h is the tunnel height relative to the airfoil profile, and c_{du} is the uncorrected wind tunnel drag coefficient.

The last correction to apply is the effect of streamline curvature. The natural curvature of free air about an immersed body is impacted by the presence of wind tunnel walls. The effect is to apparently increase the camber of the body, thus increasing the resulting lift and moment produced. As detailed in [4], the corrections for this effect on the lift and the moment coefficients are given by:

$$\begin{aligned} \Delta c_{l_{sc}} &= -\sigma c_{l_u} \\ \Delta c_{m_{\frac{1}{4}sc}} &= -\frac{\sigma}{4} \Delta c_{l_{sc}} \end{aligned}$$

where

$$\sigma = \frac{\pi^2}{48} \left(\frac{c}{h} \right)^2$$

These three effects (solid blockage, wake blockage, and streamline curvature) comprise the wall corrections to be applied to the wind tunnel data.

In summary, the corrections to be applied to the uncorrected wind tunnel data are:

$$\begin{aligned}\mathcal{E} &= \mathcal{E}_{sb} + \mathcal{E}_{wb} \\ c_l &= c_{l_u} (1 - \sigma - 2\mathcal{E}) \\ c_{d_0} &= c_{d_{0u}} (1 - 3\mathcal{E}_{sb} - 2\mathcal{E}_{wb}) \\ c_{m_{\frac{l}{4}}} &= c_{m_{\frac{l}{4u}}} (1 - 2\mathcal{E}) + \frac{\sigma c_l}{4}\end{aligned}$$

TR Section Shapes

The MSES lift predictions for the TR-4000-0050 at $Re = 1.0$ million are presented in Fig. 5. Three sets of results are depicted for transition free and transition fixed at 5% of the chord; 1) with wind tunnel walls (in tunnel), 2) unbounded flow (free air), and 3) in-tunnel results corrected for the presence of wind tunnel walls using the earlier described methodology (corrected). Comparison of the free transition and fixed transition results shows that, as expected, the lift characteristics of this airfoil are very sensitive to any forward shift in boundary-layer transition location. With transition fixed near the leading edge, the flow is mostly separated as demonstrated by the very shallow lift curve slope ($\ll 2\pi \text{ rad}^{-1}$) in the "linear" lift regime, the very low maximum lift coefficient, and the very high minimum lift coefficient. The presence of the wind tunnel walls results in increased lift with the standard corrections reducing the lift to the unbounded flow values. The fact that these corrections are accurate for the solid blockage of 10% encountered here builds confidence in the proposed wind tunnel tests as well as the numerical simulations.

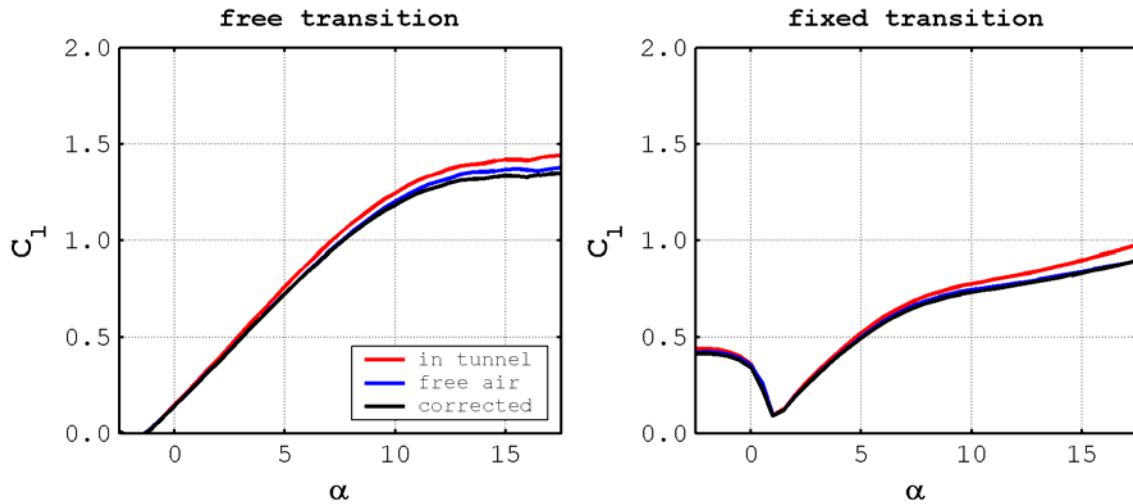


Figure 5 MSES lift predictions for TR-4000-0050 with and without wind tunnel walls at $Re = 1.0$ million and transition free and transition fixed at 5% of the chord on upper and lower surface. The lift curve labeled corrected is obtained by applying standard wind tunnel wall corrections [4] to the with wind tunnel wall results.

The OVERFLOW lift and drag predictions for the TR-4000-0050 at $Re = 1.0$ million are presented in Fig. 6 and Fig. 7, respectively. Three sets of results are depicted for transition fixed at 5% of the chord; 1) with wind tunnel walls (in tunnel), 2) unbounded flow (free air), and 3) in-tunnel results corrected for the presence of wind tunnel walls using the earlier described methodology (corrected). Laminar separation and the ensuing unsteady shedding made numerical simulations with free transition problematic at these conditions. The laminar bubble shrinks with increasing Reynolds number, and this explains that unsteady laminar bubble shedding was not an issue in previous RaNS studies of thick airfoils [2,3]. Numerical simulations of flow problems including unsteady laminar bubble shedding require an extensive gridding effort and much computational time [14]. Hence, free transition results for this airfoil will not be generated until later. Comparison of the MSES and OVERFLOW lift predictions shows excellent agreement. The presence of wind tunnel walls results in increased drag but the effect is small compared to that on the lift. Application of the standard wall corrections to the in-tunnel drag predictions leads to some discrepancies with the unbounded flow simulations. However, the effect remains small.

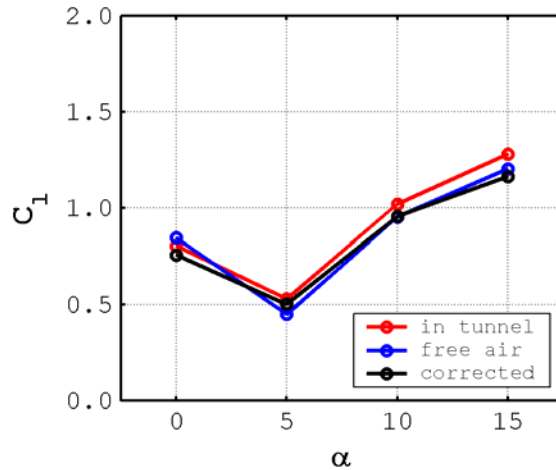


Figure 6 OVERFLOW lift predictions for TR-4000-0050 with and without wind tunnel walls at $Re = 1.0$ million and transition fixed at 5% of the chord on upper and lower surface. The lift curve labeled corrected is obtained by applying standard wind tunnel wall corrections [4] to the with wind tunnel wall results.

The MSES lift predictions for the TR-4000-1000 at $Re = 1.0$ million are presented in Fig. 8. Again, three sets of results are depicted for transition free and transition fixed at 5% of the chord; 1) with wind tunnel walls (in tunnel), 2) unbounded flow (free air), and 3) in-tunnel results corrected for the presence of wind tunnel walls using the earlier described methodology (corrected). Comparison of the free transition and fixed transition results shows that the lift characteristics of this airfoil remain sensitive to any forward shift in boundary-layer transition location. However, the negative effect of premature transition on lift is much reduced compared to the sharp trailing edge TR-4000-0050 with a

reduction in maximum lift remaining. Except near maximum lift, the standard wind tunnel correction methodology accurately predicts the effect of the walls on lift.

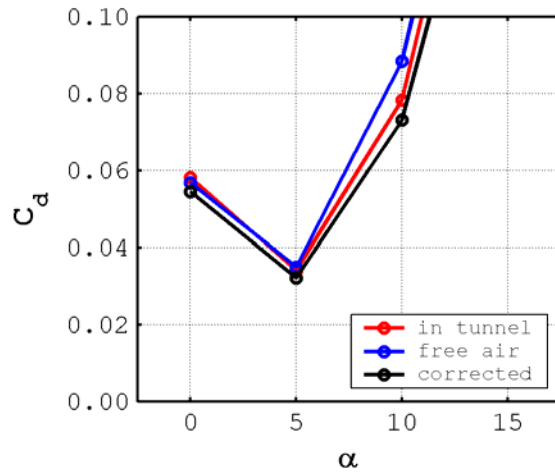


Figure 7 OVERFLOW drag predictions for TR-4000-0050 with and without wind tunnel walls at $Re = 1.0$ million and transition fixed at 5% of the chord on upper and lower surface. The lift curve labeled corrected is obtained by applying standard wind tunnel wall corrections [4] to the with wind tunnel wall results.

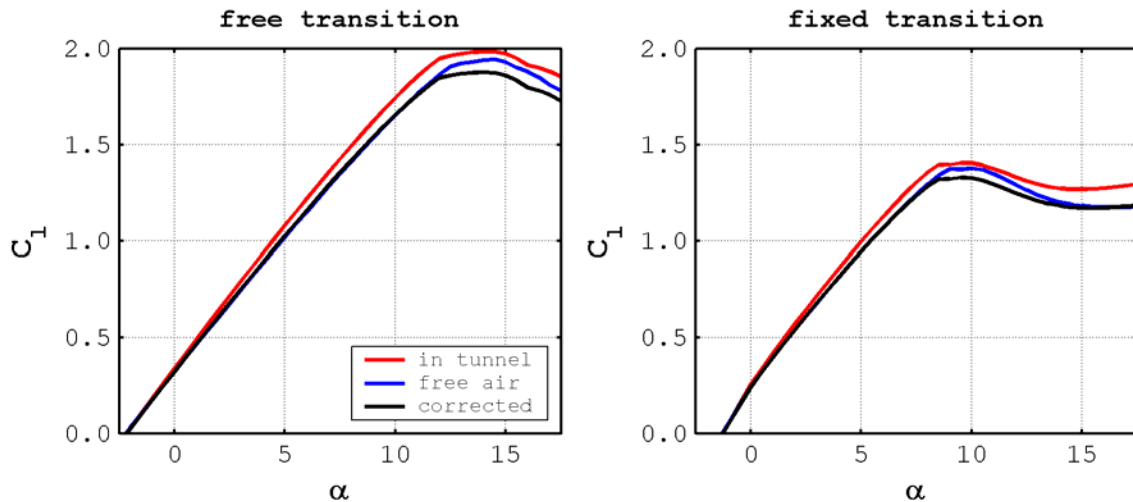


Figure 8 MSES lift predictions for TR-4000-1000 with and without wind tunnel walls at $Re = 1.0$ million and transition free and transition fixed at 5% of the chord on upper and lower surface. The lift curve labeled corrected is obtained by applying standard wind tunnel wall corrections [4] to the with wind tunnel wall results.

The OVERFLOW lift and drag predictions for the TR-4000-1000 at $Re = 1.0$ million are presented in Fig. 9 and Fig. 10, respectively. Again, three sets of results are depicted for transition free and transition fixed at 5% of the chord; 1) with wind tunnel walls (in tunnel), 2) unbounded flow (free air), and 3) in-tunnel results corrected for the presence of wind tunnel walls using the earlier described methodology (corrected). The lift results presented in Fig. 9 largely match the MSES predictions shown in Fig. 8. To limit the analysis time, an angle of attack increment of 5° was selected for the RaNS simulations. As a result, maximum lift for the free transition case is not well captured.

MSES was unable to generate converged solutions for the TR-4000-2000. This also meant that free transition information was not available for this airfoil. Instead, the transition location on the TR-4000-2000 was assumed to match that on the TR-4000-1000. The OVERFLOW lift and drag predictions for the TR-4000-2000 at $Re = 1.0$ million are presented in Fig. 11 and Fig. 12, respectively. As before, three sets of results are depicted for transition free and transition fixed at 5% of the chord; 1) with wind tunnel walls (in tunnel), 2) unbounded flow (free air), and 3) in-tunnel results corrected for the presence of wind tunnel walls using the earlier described methodology (corrected). The free transition lift and drag results without wind tunnel walls show a nonlinear behavior at low angles of attack which is caused by the existence of a laminar separation bubble on the suction surface. Changes in the pressure distribution as a result of the presence of wind tunnel walls mitigates this effect and results in a more linear performance variation with angle of attack. Still the free transition drag is higher than the fixed transition drag demonstrating the negative effect of laminar separation. Comparison of the free and fixed transition results indicates that the TR-4000-2000 lift is nominally insensitive to changes in transition location confirming the beforementioned design guideline to limit the difference between maximum thickness to chord and trailing edge thickness to chord to 20-25%.

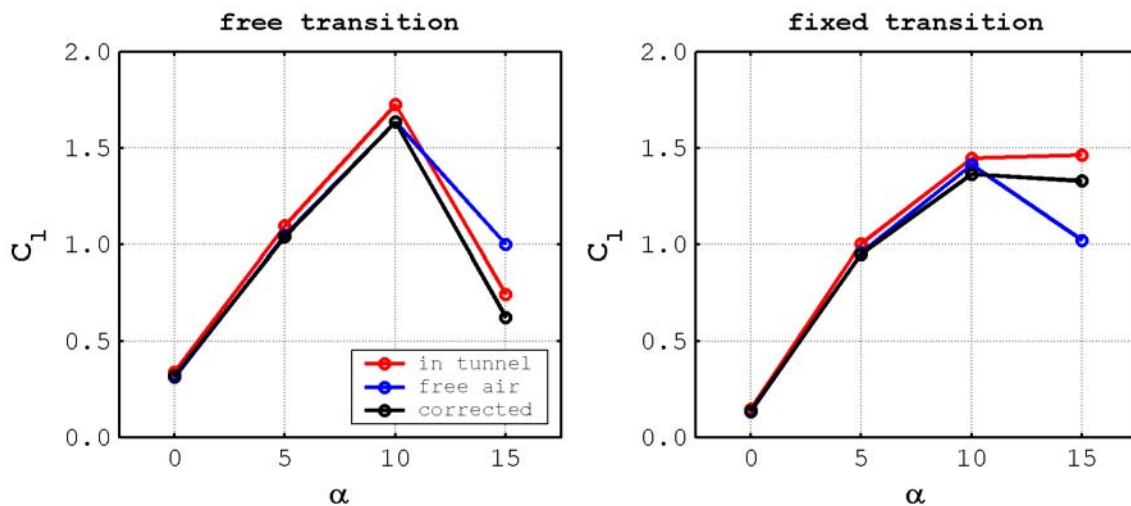


Figure 9 OVERFLOW lift predictions for TR-4000-1000 with and without wind tunnel walls at $Re = 1.0$ million and transition free and transition fixed at 5% of the chord on upper and lower surface. The lift curve labeled corrected is obtained by applying standard wind tunnel wall corrections [4] to the with wind tunnel wall results.

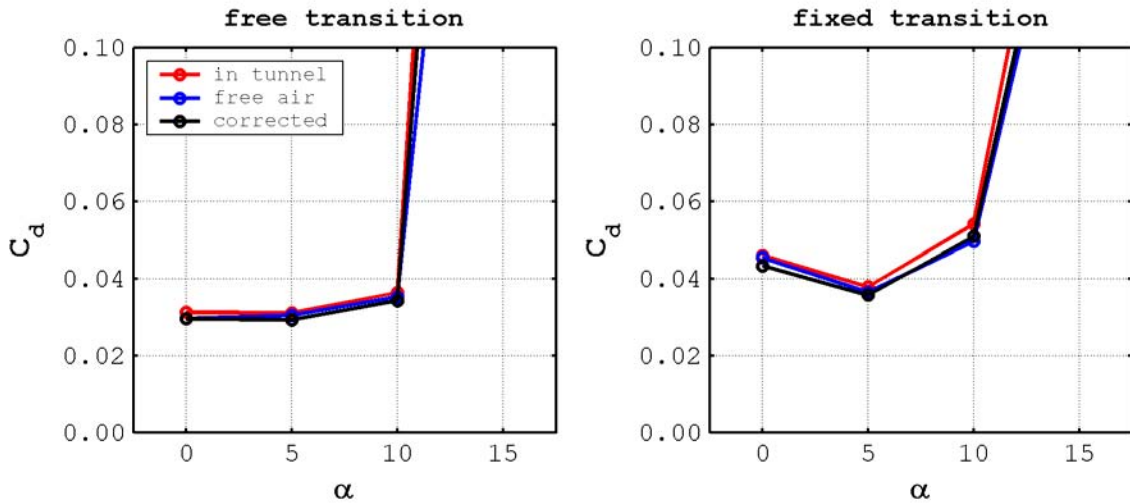


Figure 10 OVERFLOW drag predictions for TR-4000-1000 with and without wind tunnel walls at $Re = 1.0$ million and transition free and transition fixed at 5% of the chord on upper and lower surface. The lift curve labeled corrected is obtained by applying standard wind tunnel wall corrections [4] to the with wind tunnel wall results.

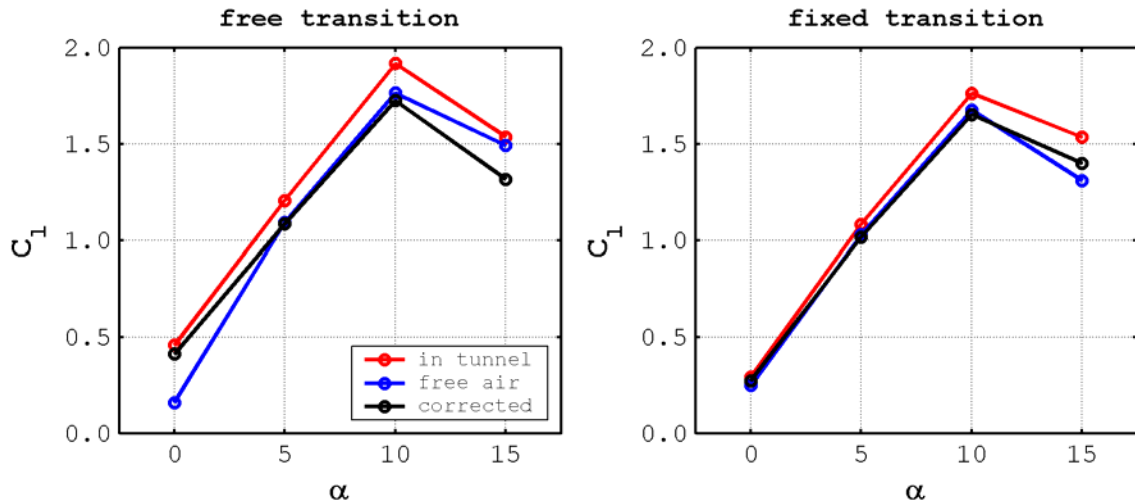


Figure 11 OVERFLOW lift predictions for TR-4000-2000 with and without wind tunnel walls at $Re = 1.0$ million and transition free and transition fixed at 5% of the chord on upper and lower surface. The lift curve labeled corrected is obtained by applying standard wind tunnel wall corrections [4] to the with wind tunnel wall results.

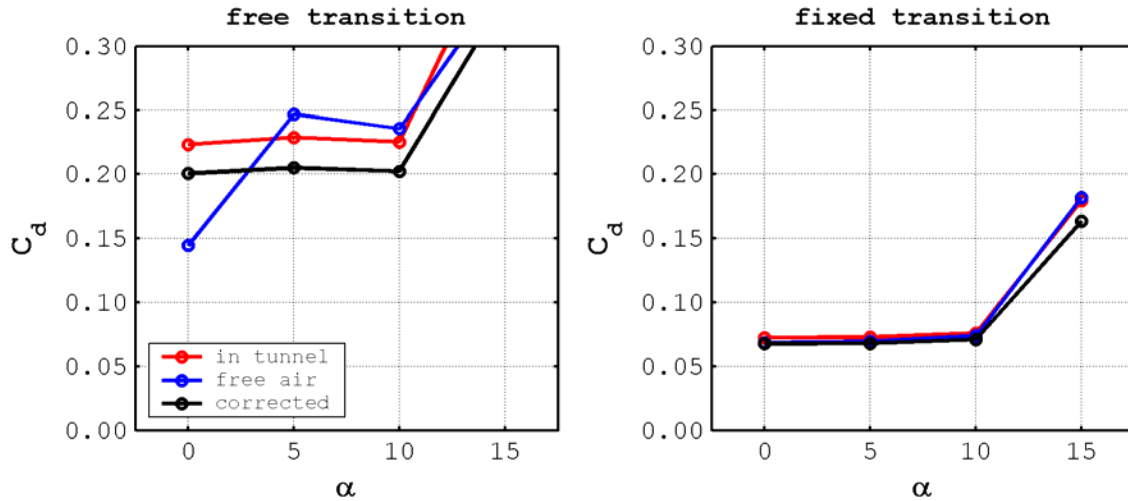


Figure 12 OVERFLOW drag predictions for TR-4000-2000 with and without wind tunnel walls at $Re = 1.0$ million and transition free and transition fixed at 5% of the chord on upper and lower surface. The lift curve labeled corrected is obtained by applying standard wind tunnel wall corrections [4] to the with wind tunnel wall results.

FB Section Shapes

In the previous section, the wind tunnel wall corrections were evaluated. Given that these corrections appear to be nominally valid for the proposed wind tunnel test of 40% maximum thickness to chord ratio airfoils at a solid blockage ratio of 10%, only unbounded flow conditions will be considered for the FB airfoils.

The MSES and ARC2D predictions for the FB-4000-0050 at $Re = 1.0$ million and transition free and transition fixed at 5% of the chord are presented in Figs. 13 and 14. Comparison of the free transition and fixed transition results shows that, as expected, the lift characteristics of this airfoil are very sensitive to any forward shift in boundary-layer transition location. Comparison of the free transition results of the FB-4000-0050 and TR-4000-0050 (Fig. 5 through 7) indicate lower lift values including a lower maximum lift coefficient for the FB-4000-0050.

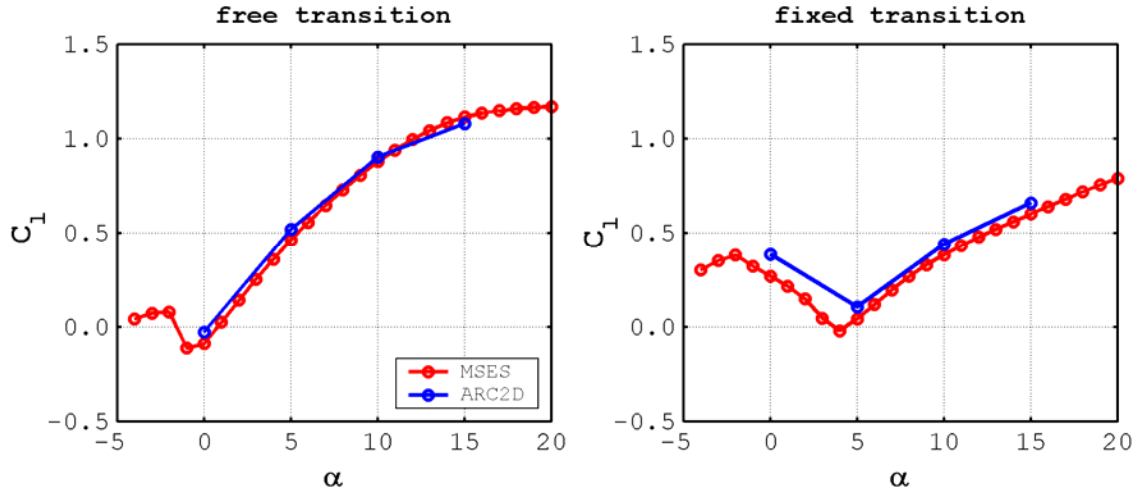


Figure 13 MSES and ARC2D lift predictions for FB-4000-0050 with transition free and transition fixed at 5% of the chord on upper and lower surface.

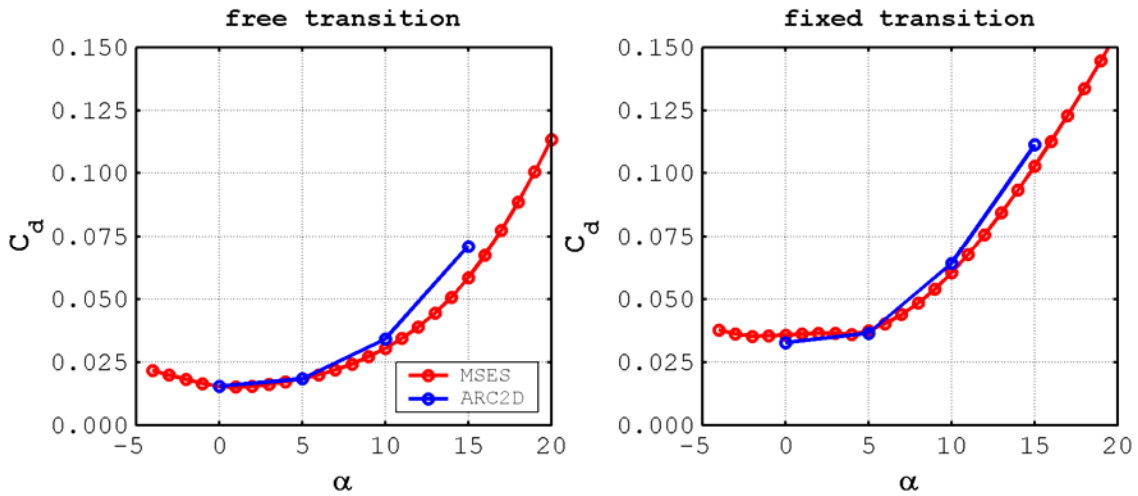


Figure 14 MSES and ARC2D drag predictions for FB-4000-0050 with transition free and transition fixed at 5% of the chord on upper and lower surface.

The MSES and ARC2D predictions for the FB-4000-1000 at $Re = 1.0$ million and transition free and transition fixed at 5% of the chord are presented in Figs. 15 and 16. Comparison of the free transition and fixed transition results shows that the lift characteristics of this airfoil remain sensitive to a forward shift in boundary-layer transition location. Comparison of the free transition results of the FB-4000-1000 and TR-4000-1000 (Figs. 8 through 10) indicate lower lift values including a lower maximum lift coefficient for the FB-4000-1000.

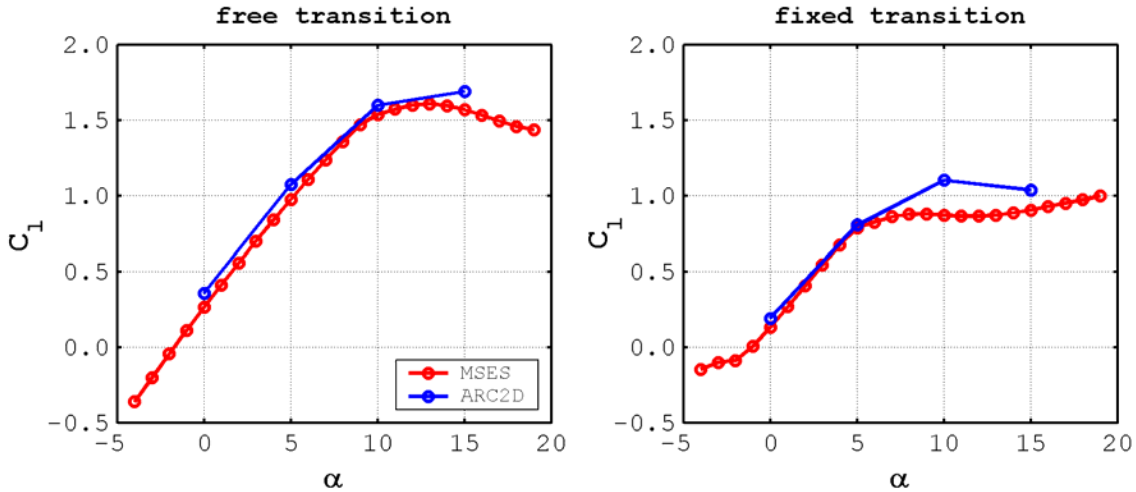


Figure 15 MSES and ARC2D lift predictions for FB-4000-1000 with transition free and transition fixed at 5% of the chord on upper and lower surface.

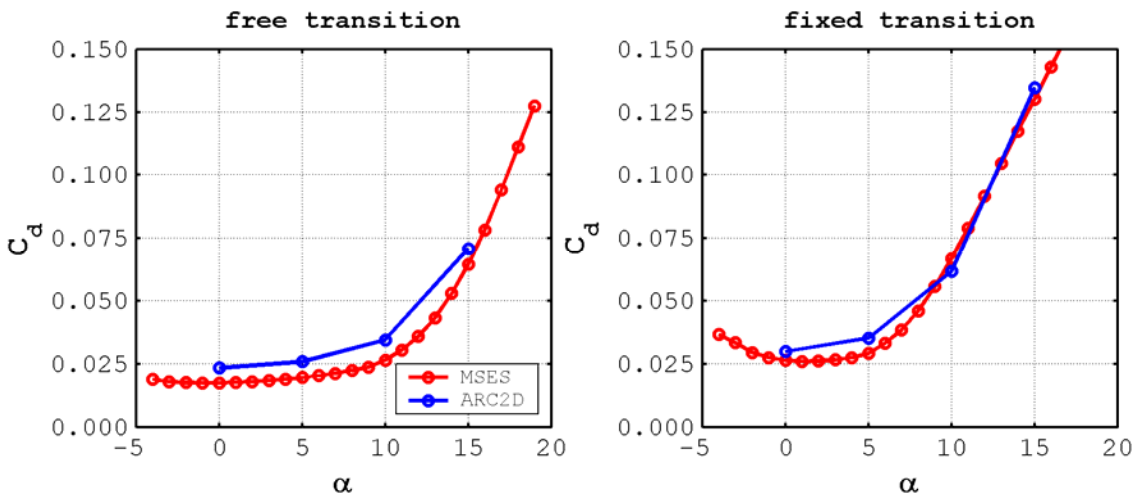


Figure 16 MSES and ARC2D drag predictions for FB-4000-1000 with transition free and transition fixed at 5% of the chord on upper and lower surface.

The ARC2D predictions for the FB-4000-2000 at $Re = 1.0$ million and transition free and transition fixed at 5% of the chord are presented in Figs. 17 and 18. This also meant that free transition information was not available for this airfoil. Instead, the transition location on the FB-4000-2000 was assumed to match that on the FB-4000-1000. The results in Fig. 17 indicate that for $\alpha = 0^\circ$ through 10° the lift is nominally unaffected by the change in transition location. However, at $\alpha = 15^\circ$ the lift results depicted in Fig. 17 differ significantly. It appears likely that the high lift value for the transition free case is an artifact caused by an incorrect transition location.

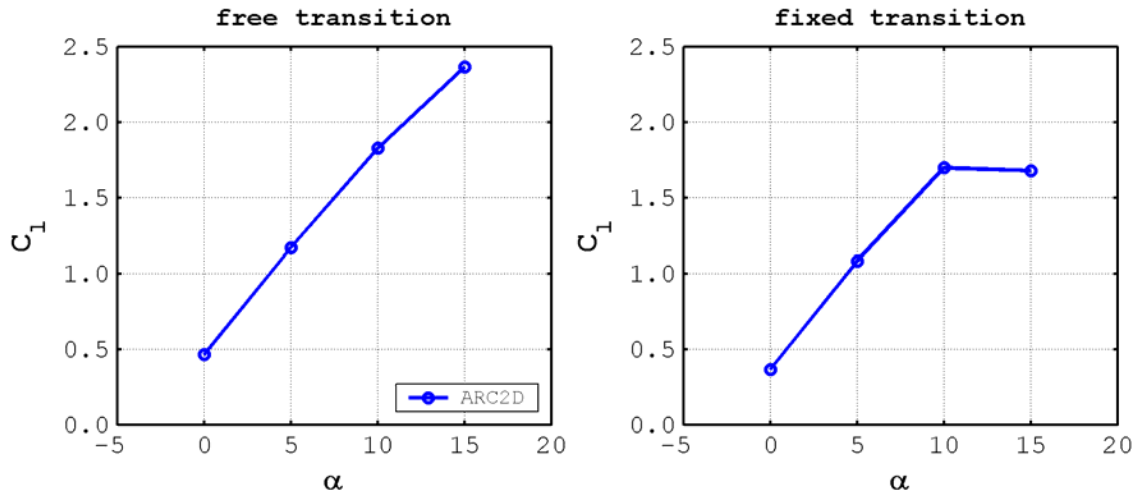


Figure 17 ARC2D lift predictions for FB-4000-2000 with transition free and transition fixed at 5% of the chord on upper and lower surface.

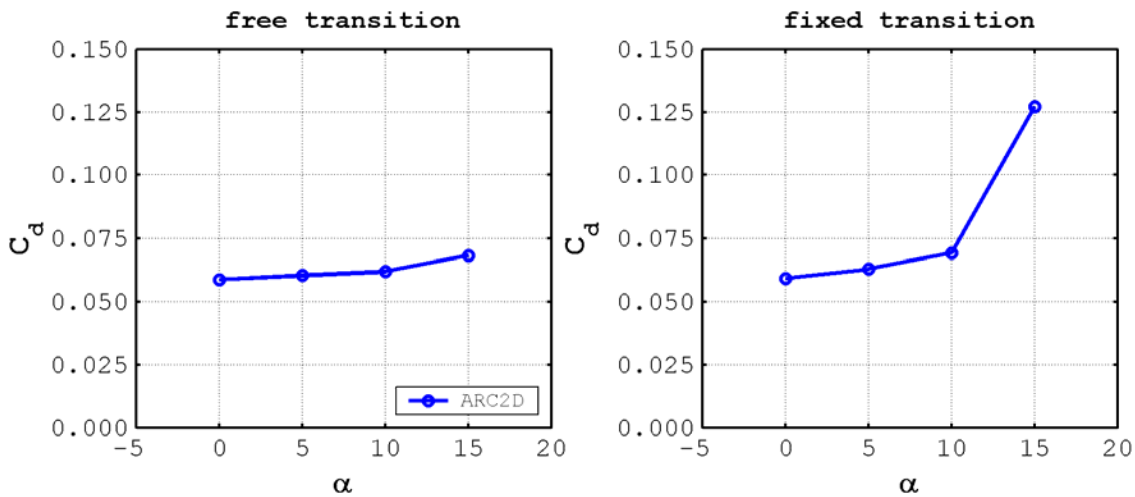


Figure 18 ARC2D drag predictions for FB-4000-2000 with transition free and transition fixed at 5% of the chord on upper and lower surface.

Discussion

Computational results for two $t/c = 40\%$ airfoil series were generated in preparation of the wind tunnel experiment on blunt trailing edge airfoils. The results for the TR airfoil family prove the standard wind tunnel corrections to be nominally valid for the proposed test of 40% maximum thickness to chord ratio airfoils at a solid blockage ratio of 10%. However, the question arises what airfoil series to test in the tunnel. The TR airfoil family presented by Standish & van Dam [3] appears to perform slightly better than the FB airfoil family presented in the final report of Phase I of the Blade System Design

Study (BSDS) [2]. The shape of the latter airfoil family is strongly governed by structural and manufacturing blade design considerations. Also the thicker versions of the FB airfoil family were never considered to have a sharp trailing edge. Hence, it is no surprise that the FB-4000-0050 has a relatively poor performance. Because the goal of this study is to validate the aerodynamic performance characteristics of flatback airfoils over a range of trailing edge thicknesses without considering specific blade design constraints, it is our recommendation to select the TR airfoil family for the wind tunnel experiment.

Conclusions

A computational fluid dynamics study of thick wind turbine section shapes considered for testing in the UC Davis wind tunnel is presented. The goals of this study were to validate standard wind tunnel wall corrections for high solid blockage conditions and to reaffirm the favorable effect of a blunt trailing edge or flatback on the performance characteristics of a representative thick airfoil shape prior to building the wind tunnel models and conducting the experiment. The numerical simulations conducted with different methodologies prove the standard wind tunnel corrections to be nominally valid for the proposed test of 40% maximum thickness to chord ratio airfoils at a solid blockage ratio of 10%. Comparison of the computed lift characteristics of the sharp trailing edge baseline airfoil and two derived flatback airfoils reaffirm the earlier observed trend of reduced sensitivity to surface contamination with increasing trailing edge thickness.

Based on the information presented in this report, the next steps are to design and manufacture three wind tunnel models and to test them in the UC Davis wind tunnel. In addition trailing edge modifications to mitigate the drag and bluff body unsteady flow separation of flatback airfoils will be researched and tested.

Table 1 TR-4000-0050 coordinates

TR-4000-0050 Coordinates			
Lower Surface		Upper Surface	
x / c	y / c	x / c	y / c
0.00000	0.00000	0.00000	0.00000
0.00001	-0.00138	0.00004	0.00324
0.00243	-0.02585	0.00037	0.00925
0.00887	-0.05202	0.00110	0.01508
0.01875	-0.07942	0.00234	0.02099
0.03169	-0.10695	0.00405	0.02699
0.04744	-0.13358	0.01212	0.04660
0.06575	-0.15839	0.02685	0.07091
0.08642	-0.18033	0.04637	0.09443
0.10958	-0.19832	0.07041	0.11646
0.13547	-0.21174	0.09866	0.13616
0.16431	-0.21999	0.13077	0.15273
0.19661	-0.22282	0.16635	0.16573
0.23260	-0.22067	0.20497	0.17503
0.27214	-0.21378	0.24620	0.18079
0.31512	-0.20240	0.28972	0.18290
0.36141	-0.18695	0.33541	0.18143
0.41080	-0.16810	0.38302	0.17678
0.46299	-0.14669	0.43215	0.16944
0.51755	-0.12367	0.48235	0.15982
0.57388	-0.10012	0.53313	0.14841
0.63118	-0.07719	0.58397	0.13570
0.68849	-0.05597	0.63430	0.12216
0.74465	-0.03742	0.68354	0.10826
0.79836	-0.02229	0.73106	0.09436
0.84823	-0.01099	0.77624	0.08084
0.89291	-0.00351	0.81848	0.06792
0.93109	0.00065	0.85715	0.05580
0.96165	0.00183	0.89164	0.04440
0.98346	0.00049	0.92166	0.03337
0.99601	-0.00160	0.94740	0.02284
1.00000	-0.00250	0.96886	0.01375
		0.98550	0.00715
		0.99625	0.00354
		1.00000	0.00250

Table 2 TR-4000-1000 coordinates

TR-4000-1000 Coordinates			
Lower Surface		Upper Surface	
x / c	y / c	x / c	y / c
0.00000	0.00000	0.00000	0.00000
0.00001	-0.00135	0.00004	0.00319
0.00243	-0.02545	0.00037	0.00908
0.00887	-0.05129	0.00110	0.01481
0.01876	-0.07839	0.00234	0.02060
0.03169	-0.10564	0.00405	0.02649
0.04744	-0.13206	0.01212	0.04576
0.06575	-0.15673	0.02685	0.06969
0.08642	-0.17860	0.04637	0.09293
0.10958	-0.19663	0.07041	0.11477
0.13547	-0.21021	0.09866	0.13444
0.16432	-0.21876	0.13076	0.15116
0.19661	-0.22206	0.16635	0.16453
0.23260	-0.22057	0.20497	0.17442
0.27214	-0.21457	0.24620	0.18098
0.31513	-0.20431	0.28972	0.18413
0.36141	-0.19025	0.33541	0.18393
0.41080	-0.17311	0.38301	0.18080
0.46299	-0.15374	0.43215	0.17525
0.51755	-0.13312	0.48235	0.16769
0.57388	-0.11238	0.53313	0.15860
0.63118	-0.09265	0.58397	0.14850
0.68849	-0.07502	0.63430	0.13780
0.74465	-0.06041	0.68354	0.12698
0.79836	-0.04947	0.73106	0.11636
0.84823	-0.04248	0.77624	0.10625
0.89291	-0.03924	0.81848	0.09679
0.93109	-0.03901	0.85715	0.08811
0.96165	-0.04120	0.89164	0.08000
0.98346	-0.04506	0.92166	0.07203
0.99601	-0.04862	0.94740	0.06428
1.00000	-0.05000	0.96886	0.05760
		0.98550	0.05293
		0.99625	0.05060
		1.00000	0.05000

Table 3 TR-4000-2000 coordinates

TR-4000-2000 Coordinates			
Lower Surface		Upper Surface	
x / c	y / c	x / c	y / c
0.00000	0.00000	0.00000	0.00000
0.00001	-0.00132	0.00004	0.00312
0.00243	-0.02501	0.00037	0.00890
0.00887	-0.05048	0.00110	0.01450
0.01876	-0.07722	0.00234	0.02016
0.03169	-0.10418	0.00405	0.02593
0.04744	-0.13035	0.01212	0.04482
0.06575	-0.15484	0.02685	0.06833
0.08642	-0.17662	0.04637	0.09123
0.10958	-0.19468	0.07041	0.11285
0.13547	-0.20841	0.09866	0.13246
0.16432	-0.21727	0.13076	0.14933
0.19662	-0.22106	0.16634	0.16306
0.23261	-0.22027	0.20497	0.17357
0.27215	-0.21519	0.24620	0.18098
0.31513	-0.20612	0.28972	0.18521
0.36141	-0.19355	0.33540	0.18636
0.41080	-0.17821	0.38301	0.18486
0.46299	-0.16101	0.43215	0.18120
0.51755	-0.14294	0.48235	0.17582
0.57388	-0.12516	0.53313	0.16920
0.63118	-0.10882	0.58397	0.16185
0.68849	-0.09499	0.63430	0.15417
0.74465	-0.08455	0.68354	0.14661
0.79836	-0.07804	0.73106	0.13944
0.84823	-0.07560	0.77624	0.13293
0.89291	-0.07682	0.81848	0.12714
0.93109	-0.08075	0.85715	0.12208
0.96165	-0.08650	0.89164	0.11745
0.98346	-0.09300	0.92166	0.11271
0.99601	-0.09812	0.94740	0.10789
1.00000	-0.10000	0.96886	0.10376
		0.98550	0.10112
		0.99625	0.10013
		1.00000	0.10000

Table 4 FB-4000-0050 coordinates.

FB-4000-0050 Coordinates			
Lower Surface		Upper Surface	
x / c	y / c	x / c	y / c
0.00000	0.00000	0.00000	0.00000
0.00149	-0.02058	0.00149	0.01946
0.00597	-0.04149	0.00597	0.03765
0.01340	-0.06175	0.01340	0.05519
0.02376	-0.08054	0.02376	0.07266
0.03699	-0.09765	0.03699	0.09036
0.05303	-0.11336	0.05303	0.10812
0.07181	-0.12802	0.07181	0.12541
0.09324	-0.14167	0.09324	0.14161
0.11722	-0.15406	0.11722	0.15626
0.14363	-0.16496	0.14363	0.16916
0.17234	-0.17435	0.17234	0.18024
0.20321	-0.18227	0.20321	0.18942
0.23611	-0.18866	0.23611	0.19650
0.27085	-0.19331	0.27085	0.20122
0.30727	-0.19594	0.30727	0.20340
0.34520	-0.19649	0.34520	0.20303
0.38443	-0.19499	0.38443	0.20029
0.42476	-0.19142	0.42476	0.19544
0.46598	-0.18552	0.46598	0.18865
0.50787	-0.17693	0.50787	0.18002
0.55021	-0.16542	0.55021	0.16962
0.59273	-0.15106	0.59273	0.15761
0.63521	-0.13425	0.63521	0.14432
0.67736	-0.11558	0.67736	0.13014
0.71893	-0.09579	0.71893	0.11540
0.75961	-0.07576	0.75961	0.10025
0.79909	-0.05635	0.79909	0.08479
0.83703	-0.03841	0.83703	0.06922
0.87305	-0.02280	0.87305	0.05398
0.90669	-0.01067	0.90669	0.03967
0.93741	-0.00306	0.93741	0.02686
0.96443	-0.00020	0.96443	0.01600
0.98650	-0.00086	0.98650	0.00749
1.00000	-0.00250	1.00000	0.00250

Table 5 FB-4000-1000 coordinates.

FB-4000-1000 Coordinates			
Lower Surface		Upper Surface	
x / c	y / c	x / c	y / c
0.00000	0.00000	0.00000	0.00000
0.00149	-0.02058	0.00149	0.01946
0.00597	-0.04149	0.00597	0.03765
0.01340	-0.06175	0.01340	0.05519
0.02376	-0.08054	0.02376	0.07266
0.03699	-0.09765	0.03699	0.09036
0.05303	-0.11336	0.05303	0.10812
0.07181	-0.12802	0.07181	0.12541
0.09324	-0.14167	0.09324	0.14161
0.11722	-0.15406	0.11722	0.15626
0.14363	-0.16496	0.14363	0.16916
0.17234	-0.17435	0.17234	0.18024
0.20321	-0.18227	0.20321	0.18942
0.23611	-0.18866	0.23611	0.19650
0.27085	-0.19331	0.27085	0.20122
0.30727	-0.19594	0.30727	0.20340
0.34520	-0.19651	0.34520	0.20305
0.38443	-0.19512	0.38443	0.20042
0.42476	-0.19184	0.42476	0.19585
0.46598	-0.18652	0.46598	0.18965
0.50787	-0.17891	0.50787	0.18200
0.55021	-0.16885	0.55021	0.17305
0.59273	-0.15650	0.59273	0.16305
0.63521	-0.14226	0.63521	0.15232
0.67736	-0.12669	0.67736	0.14126
0.71893	-0.11050	0.71893	0.13011
0.75961	-0.09445	0.75961	0.11894
0.79909	-0.07928	0.79909	0.10771
0.83703	-0.06568	0.83703	0.09650
0.87305	-0.05440	0.87305	0.08558
0.90669	-0.04641	0.90669	0.07541
0.93741	-0.04265	0.93741	0.06646
0.96443	-0.04320	0.96443	0.05900
0.98650	-0.04665	0.98650	0.05328
1.00000	-0.05000	1.00000	0.05000

Table 6 FB-4000-2000 coordinates.

FB-4000-2000 Coordinates			
Lower Surface		Upper Surface	
x / c	y / c	x / c	y / c
0.00000	0.00000	0.00000	0.00000
0.00149	-0.02058	0.00149	0.01946
0.00597	-0.04149	0.00597	0.03765
0.01340	-0.06175	0.01340	0.05519
0.02376	-0.08054	0.02376	0.07266
0.03699	-0.09765	0.03699	0.09036
0.05303	-0.11336	0.05303	0.10812
0.07181	-0.12802	0.07181	0.12541
0.09324	-0.14167	0.09324	0.14161
0.11722	-0.15406	0.11722	0.15626
0.14363	-0.16496	0.14363	0.16916
0.17234	-0.17435	0.17234	0.18024
0.20321	-0.18227	0.20321	0.18942
0.23611	-0.18866	0.23611	0.19650
0.27085	-0.19331	0.27085	0.20122
0.30727	-0.19594	0.30727	0.20340
0.34520	-0.19653	0.34520	0.20307
0.38443	-0.19525	0.38443	0.20055
0.42476	-0.19228	0.42476	0.19629
0.46598	-0.18757	0.46598	0.19070
0.50787	-0.18099	0.50787	0.18408
0.55021	-0.17247	0.55021	0.17667
0.59273	-0.16222	0.59273	0.16877
0.63521	-0.15068	0.63521	0.16075
0.67736	-0.13840	0.67736	0.15296
0.71893	-0.12599	0.71893	0.14560
0.75961	-0.11412	0.75961	0.13861
0.79909	-0.10341	0.79909	0.13184
0.83703	-0.09439	0.83703	0.12521
0.87305	-0.08765	0.87305	0.11883
0.90669	-0.08404	0.90669	0.11304
0.93741	-0.08433	0.93741	0.10813
0.96443	-0.08846	0.96443	0.10426
0.98650	-0.09485	0.98650	0.10149
1.00000	-0.10000	1.00000	0.10000

References

- 1 TPI Composites, "Innovative Design Approaches for Large Wind Turbine Blades," SAND2003-0723, March 2003.
- 2 TPI Composites, "Innovative Design Approaches for Large Wind Turbine Blades – Final Report," SAND2004-0074, 2004.
- 3 Standish, K.J., and van Dam, C.P., "Aerodynamic Analysis of Blunt Trailing Edge Airfoils," *Journal of Solar Energy Engineering*, Vol. 125, Nov. 2003, pp. 479-487.
- 4 Barlow, J.B., Rae, W.H., and Pope, A., Low-Speed Wind Tunnel Testing, 3rd Edition, Wiley, 1999.
- 5 Drela, M., "Newton Solution of Coupled Viscous/Inviscid Multi-Element Airfoil Flows," AIAA Paper 90-1470, June 1990.
- 6 Drela, M., "Integral Boundary Layer Formulation for Blunt Trailing Edges," AIAA Paper 89-2166, July-Aug. 1989.
- 7 Pulliam, T.H., "Efficient Solution Methods for the Navier-Stokes Equations," Lecture Notes for the von Kármán Institute for Fluid Dynamics Lecture Series: Numerical Techniques for Viscous Flow Computation in Turbomachinery Bladings, von Kármán Institute, Rhode-St-Genese, Belgium, 1985.
- 8 Pulliam, T.H., "Time Accuracy and the Use of Implicit Methods," AIAA Paper 93-3360, Presented at AIAA Computational Fluid Dynamics Conference, Orlando, FL, July 1993.
- 9 Beam, R., and Warming, R.F., "An Implicit Finite-Difference Algorithm for Hyperbolic Systems in Conservation Law Form," *Journal of Computational Physics*, Vol. 22, Sep. 1976, pp. 87-110.
- 10 Chao, D.D., and van Dam, C.P., "Airfoil Drag Prediction and Decomposition," *Journal of Aircraft*, Vol. 36, No. 4, July-Aug. 1999, pp. 675-681.
- 11 Barth, T.J., Pulliam, T.H., and Buning, P.G., "Navier-Stokes Computations for Exotic Airfoils," AIAA Paper 85-0109, Jan. 1985.
- 12 Zingg, D.W., "Low Mach Number Euler Computations," *Canadian Aeronautics and Space Journal*, Vol. 36, No. 3, Sep. 1990, pp. 146-152.

- 13 Buning, P.G., Jespersen, D.C., Pulliam, T.H., Klopfer, G.H., Chan, W.M., Slotnick, J.P., Krist, S.E., and Renze, K.J., "Overflow User's Manual 1.8aa," NASA Langley Research Center, April 24, 2003.
- 14 Mayda, E.A., and van Dam, C.P., "Bubble-Induced Unsteadiness on a Wind Turbine Airfoil," *Journal of Solar Energy Engineering*, Vol. 124, Nov. 2002, pp. 335-344.
- 15 Spalart, P.R., and Allmaras, S.R., "A One-Equation Turbulence Model for Aerodynamic Flows," *La Recherche Aéronautique*, No. 1, 1994, pp. 5-21.
- 16 Menter, F. R., "Two-Equation Eddy-Viscosity Turbulence Models for Engineering Applications," *AIAA Journal*, Vol. 32, No. 8, 1994, pp. 1598-1605.
- 17 Chan, W.M., Rogers, S.E., Nash, S.M., Buning, P.G., and Meakin, R.L., "User's Manual for Chimera Grid Tools, Version 1.8," NASA Ames Research Center, May, 2003. (available as of July 2004 at <http://people.nas.nasa.gov/~rogers/cgt/doc/man.html>)

DISTRIBUTION:

Tom Acker
Northern Arizona University
PO Box 15600
Flagstaff, AZ 86011-5600

Ian Baring-Gould
NREL/NWTC
1617 Cole Boulevard MS 3811
Golden, CO 80401

Keith Bennett
U.S. Department of Energy
Golden Field Office
1617 Cole Boulevard
Golden, CO 80401-3393

Karl Bergey
University of Oklahoma
Aerospace Engineering Dept.
Norman, OK 73069

Mike Bergey
Bergey Wind Power Company
2200 Industrial Blvd.
Norman, OK 73069

Derek Berry
TPI Composites, Inc.
373 Market Street
Warren, RI 02885-0328

Gunjit Bir
NREL/NWTC
1617 Cole Boulevard MS 3811
Golden, CO 80401

Marshall Buhl
NREL/NWTC
1617 Cole Boulevard MS 3811
Golden, CO 80401

C.P. Sandy Butterfield
NREL/NWTC
1617 Cole Boulevard MS 3811
Golden, CO 80401

Garrett Bywaters
Northern Power Systems
182 Mad River Park
Waitsfield, VT 05673

Doug Cairns
Montana State University
Dept. of Mechanical & Industrial Eng.
College of Engineering
PO Box 173800
Bozeman, MT 59717-3800

David Calley
Southwest Windpower
1801 West Route 66
Flagstaff, AZ 86001

Larry Carr
NASA Ames Research Center
24285 Summerhill Ave.
Los Altos, CA 94024

Jamie Chapman
Texas Tech University
Wind Science & Eng. Research Center
Box 41023
Lubbock, TX 79409-1023

Kip Cheney
PO Box 456
Middlebury, CT 06762

Craig Christensen
Clipper Windpower Technology, Inc.
6305 Carpinteria Ave. Suite 300
Carpinteria, CA 93013

R. Nolan Clark
USDA - Agricultural Research Service
PO Drawer 10
Bushland, TX 79012

Trudy Forsyth
NREL/NWTC
1617 Cole Boulevard
Golden, CO 80401

C. Cohee
Foam Matrix, Inc.
1123 E. Redondo Blvd.
Inglewood, CA 90302

Brian Glenn
Clipper Windpower Technology, Inc.
6305 Carpinteria Ave. Suite 300
Carpinteria, CA 93013

Joe Cohen
Princeton Economic Research, Inc.
1700 Rockville Pike, Suite 550
Rockville, MD 20852

R. Gopalakrishnan
GE Wind Energy
GTTC, 300 Garlington Road
Greenville, SC 29602

C. Jito Coleman
Northern Power Systems
182 Mad River Park
Waitsfield, VT 05673

Dayton Griffin
Global Energy Concepts, LLC
1809 7th Ave., Suite 900
Seattle, WA 98101

Ken J. Deering
The Wind Turbine Company
PO Box 40569
Bellevue, WA 98015-4569

Maureen Hand
NREL/NWTC
1617 Cole Boulevard MS 3811
Golden, CO 80401

James Dehlsen
Clipper Windpower Technology, Inc.
6305 Carpinteria Ave. Suite 300
Carpinteria, CA 93013

Thomas Hermann
Odonata Research
202 Russell Ave. S.
Minneapolis, MN 55405-1932

Edgar DeMeo
Renewable Energy Consulting Services
2791 Emerson St.
Palo Alto, CA 94306

D. Hodges
Georgia Institute of Technology
270 Ferst Drive
Atlanta, GA 30332

S. Finn
GE Global Research
One Research Circle
Niskayuna, NY 12309

William E. Holley
GE Wind Energy
GTTC, M/D 100D
300 Garlington Rd.
PO Box 648
Greenville, SC 29602-0648

Peter Finnegan
GE Global Research
One Research Circle
Niskayuna, NY 12309

Adam Holman
USDA - Agricultural Research Service
PO Drawer 10
Bushland, TX 79012-0010

D.M. Hoyt
NSE Composites
1101 N. Northlake Way, Suite 4
Seattle, WA 98103

Scott Hughes
NREL/NWTC
1617 Cole Boulevard MS 3911
Golden, CO 80401

Kevin Jackson
Dynamic Design
123 C Street
Davis, CA 95616

Eric Jacobsen
GE Wind Energy - GTTC
300 Garlington Rd.
Greenville, SC 29602

George James
Structures & Dynamics Branch Mail Code
ES2
NASA Johnson Space Center
2101 NASA Rd 1
Houston, TX 77058

Jason Jonkman
NREL/NWTC
1617 Cole Boulevard
Golden, CO 80401

Gary Kanaby
Knight & Carver Yacht Center
1313 Bay Marina Drive
National City, CA 91950

Benjamin Karlson
Wind Energy Technology Department
Room 5H-088
1000 Independence Ave. S.W.
Washington, DC 20585

Jason Kiddy
Aither Engineering, Inc.
4865 Walden Lane
Lanham, MD 20706

M. Kramer
Foam Matrix, Inc.
PO Box 6394
Malibu, CA 90264

David Laino
Windward Engineering
8219 Glen Arbor Dr.
Rosedale, MD 21237-3379

Scott Larwood
1120 N. Stockton St.
Stockton, CA 95203

Bill Leighty
Alaska Applied Sciences, Inc.
PO Box 20993
Juneau, AK 99802-0993

Wendy Lin
GE Global Research
One Research Circle
Niskayuna, NY 12309

Steve Lockard
TPI Composites, Inc.
373 Market Street
Warren, RI 02885-0367

James Locke
AIRBUS North America Eng., Inc.
213 Mead Street
Wichita, KS 67202

James Lyons
Novus Energy Partners
201 North Union St., Suite 350
Alexandria, VA 22314

David Malcolm
Global Energy Concepts, LLC
1809 7th Ave., Suite 900
Seattle, WA 98101

John F. Mandell
Montana State University
302 Cableigh Hall
Bozeman, MT 59717

Tim McCoy
Global Energy Concepts, LLC
1809 7th Ave., Suite 900
Seattle, WA 98101

L. McKittrick
Montana State University
Dept. of Mechanical & Industrial Eng.
220 Roberts Hall
Bozeman, MT 59717

Amir Mikhail
Clipper Windpower Technology, Inc.
6305 Carpinteria Ave. Suite 300
Carpinteria, CA 93013

Patrick Moriarty
NREL/NWTC
1617 Cole Boulevard
Golden, CO 80401

Walt Musial
NREL/NWTC
1617 Cole Boulevard MS 3811
Golden, CO 80401

Library (5) NWTC
NREL/NWTC
1617 Cole Boulevard
Golden, CO 80401

Byron Neal
USDA - Agricultural Research Service
PO Drawer 10
Bushland, TX 79012

Steve Nolet
TPI Composites, Inc.
373 Market Street
Warren, RI 02885-0328

Richard Osgood
NREL/NWTC
1617 Cole Boulevard
Golden, CO 80401

Tim Olsen
Tim Olsen Consulting
1428 S. Humboldt St.
Denver, CO 80210

Robert Z. Poore
Global Energy Concepts, LLC
1809 7th Ave., Suite 900
Seattle, WA 98101

Cecelia M. Poshedly (5)
Office of Wind & Hydropower Technologies
EE-2B Forrestal Building
U.S. Department of Energy
1000 Independence Ave. SW
Washington, DC 20585

Robert Preus
Abundant Renewable Energy
22700 NE Mountain Top Road
Newberg, OR 97132

Jim Richmond
MDEC
3368 Mountain Trail Ave.
Newberg Park, CA 91320

Michael Robinson
NREL/NWTC
1617 Cole Boulevard
Golden, CO 80401

Dan Sanchez
U.S. Department of Energy
NNSA/SSO
PO Box 5400 MS 0184
Albuquerque, NM 87185-0184

Scott Schreck
NREL/NWTC
1617 Cole Boulevard MS 3811
Golden, CO 80401

David Simms
NREL/NWTC
1617 Cole Boulevard MS 3811
Golden, CO 80401

Brian Smith
NREL/NWTC
1617 Cole Boulevard MS 3811
Golden, CO 80401

J. Sommer
Molded Fieber Glass Companies/West
9400 Holly Road
Adelanto, CA 92301

Ken Starcher
Alternative Energy Institute
West Texas A & M University
PO Box 248
Canyon, TX 79016

Fred Stoll
Webcore Technologies
8821 Washington Church Rd.
Miamisburg, OH 45342

Herbert J. Sutherland
HJS Consulting
1700 Camino Gusto NW
Albuquerque, NM 87107-2615

Andrew Swift
Texas Tech University
Civil Engineering
PO Box 41023
Lubbock, TX 79409-1023

J. Thompson
ATK Composite Structures
PO Box 160433 MS YC14
Clearfield, UT 84016-0433

Robert W. Thresher
NREL/NWTC
1617 Cole Boulevard MS 3811
Golden, CO 80401

Steve Tsai
Stanford University
Aeronautics & Astronautics
Durand Bldg. Room 381
Stanford, CA 94305-4035

William A. Vachon
W. A. Vachon & Associates
PO Box 149
Manchester, MA 01944

C.P. van Dam (10)
Dept. of Mechanical & Aerospace Eng.
University of California, Davis
One Shields Avenue
Davis, CA 95616-5294

Jeroen van Dam
Windward Engineering
NREL/NWTC
1617 Cole Boulevard
Golden, CO 80401

Brian Vick
USDA - Agricultural Research Service
PO Drawer 10
Bushland, TX 79012

Carl Weinberg
Weinberg & Associates
42 Green Oaks Court
Walnut Creek, CA 94596-5808

Kyle Wetzel
Wetzel Engineering, Inc.
PO Box 4153
Lawrence, KS 66046-1153

Mike Zuteck
MDZ Consulting
601 Clear Lake Road
Clear Lake Shores, TX 77565

INTERNAL DISTRIBUTION:

MS 0557 D.T. Griffith, 1524
MS1124 J.R. Zayas, 6333
MS 1124 T.D. Ashwill, 6333
MS 1124 M.E. Barone, 01515
MS 1124 D.E. Berg, 6333 (10)
MS 1124 S.M. Gershin, 6333
MS 1124 R.R. Hill, 6333
MS 1124 W. Johnson, 6333
MS 1124 D.L. Laird, 6333
MS 1124 D.W. Lobitz, 6333
MS 1124 J. Paquette, 6333
MS 1124 M.A. Rumsey, 6333
MS 1124 J. Stinebaugh, 6333
MS 1124 P.S. Veers, 6333
MS 0899 Technical Library, 9536
(Electronic)

